

RESEARCH AND ANALYSIS

Characterization of Emissions from a Desktop 3D Printer

Luís Mendes,^{1,4,5} Anneli Kangas,² Kirsi Kukko,³ Bjarke Mølgaard,¹ Arto Säämänen,² Tomi Kanerva,² Iñigo Flores Ituarte,³ Marika Huhtiniemi,² Helene Stockmann-Juvala,² Jouni Partanen,³ Kaarle Hämeri,¹ Konstantinos Eleftheriadis,⁴ and Anna-Kaisa Viitanen²

¹Department of Physics, Division of Atmospheric Sciences, University of Helsinki, Helsinki, Finland

²Finnish Institute of Occupational Health, Helsinki, Finland


³Department of Mechanical Engineering, Aalto University, Espoo, Finland

⁴Institute of Nuclear and Radiological Sciences and Technology, Energy and Safety – Environmental Radioactivity Laboratory, N.C.S.R. “Demokritos”, Athens, Greece

⁵Department of Environment, University of the Aegean, Mytilene, Greece

Keywords:

3D printing
gas phase compounds
industrial ecology
material extrusion
nanoparticles
occupational health

 Supporting information is linked to this article on the JIE website

Summary

3D printers are currently widely available and very popular among the general public. However, the use of these devices may pose health risks to users, attributable to air-quality issues arising from gaseous and particulate emissions in particular. We characterized emissions from a low-end 3D printer based on material extrusion, using the most common polymers: acrylonitrile-butadiene-styrene (ABS) and polylactic acid (PLA). Measurements were carried out in an emission chamber and a conventional room. Particle emission rates were obtained by direct measurement and modeling, whereas the influence of extrusion temperature was also evaluated. ABS was the material with the highest aerosol emission rate. The nanoparticle emission ranged from $3.7 \cdot 10^8$ to $1.4 \cdot 10^9$ particles per second ($\# \text{ s}^{-1}$) in chamber measurements and from $2.0 \cdot 10^9$ to $4.0 \cdot 10^9$ $\# \text{ s}^{-1}$ in room measurements, when the recommended extruder temperature was used. Printing with PLA emitted nanoparticles at the rate of $1.0 \cdot 10^7$ $\# \text{ s}^{-1}$ inside the chamber and negligible emissions in room experiments. Emission rates were observed to depend strongly on extruder temperature. The particles' mean size ranged from 7.8 to 10.5 nanometers (nm). We also detected a significant emission rate of particles of 1 to 3 nm in size during all printing events. The amounts of volatile organic and other gaseous compounds were only traceable and are not expected to pose health risks. Our study suggests that measures preventing human exposure to high nanoparticle concentrations should be adopted when using low-end 3D printers.

Introduction

Additive manufacturing (AM), commonly known as 3D printing when referring to low-end AM machines in nontechnical terms (ISO/ASTM 2015), has been under development

for over 30 years. Nevertheless, attention from industry, policy makers, research institutes, the general public, and the media is currently at an all-time high (Caffrey and Wohlers 2014). With hundreds of small start-up companies around the world

Conflict of interest statement: The authors have no conflict to declare.

Address correspondence to: Anna-Kaisa Viitanen, Finnish Institute of Occupational Health, P.O. Box 40, FI-00251 Helsinki, Finland. Email: anna-kaisa.viitanen@ttl.fi; Web: www.ttl.fi

© 2017 The Authors. Journal of Industrial Ecology, published by Wiley Periodicals, Inc., on behalf of Yale University. This is an open access article under the terms of the Creative Commons Attribution License, which permits use, distribution and reproduction in any medium, provided the original work is properly cited.
DOI: 10.1111/jiec.12569

Editor managing review: Martin Baumers

Volume 21, Number S1

supplying low-cost equipment for educational, professional, and recreational purposes, 3D printing is now more readily available to the general public than ever before.

The main technology used in low-end AM machines, generally called 3D printers, is the material extrusion (ME), in which a thermoplastic material is selectively dispensed through a nozzle or orifice to build parts from 3D model data, layer upon layer, so that a functional object is created (ISO/ASTM 2015). This technology uses polymer filaments as feedstock. Acrylonitrile butadiene styrene (ABS) and polylactic acid (PLA) are the most commonly used materials (Bumgarner 2013; Stephens et al. 2013).

The use of 3D printers in nontraditional manufacturing environments may lead to new groups of people being exposed to hazardous emissions, such as harmful dusts and chemicals. These users may not be adequately trained or have appropriate facilities for operating this type of systems (Bradbrook et al. 2013). An increasing number of people may be exposed to particles and chemicals released during the application of ME technology in offices, hobbyist environments, homes, or schools. Health concerns may arise regarding the particulate and gaseous emissions from ME, especially given that the typical design of low-end AM machines has no built-in containment or air cleaning system. Such features are available usually in more advanced and expensive AM machines.

Previous research has shown that thermal processing of polymer materials is likely to produce airborne contaminants, including carcinogens and respiratory irritants (HSE 2002; Sims et al. 1994; Dematteo 2011) as well as particulate matter. The composition of the fume generated by plastic heating may be complex and vary depending on type of plastic, formulation, and processing conditions (Unwin et al. 2013).

Several scientific studies have identified adverse health effects of nanoparticles (i.e., particles smaller than 100 nanometers [nm]) (Pope and Dockery 2006; Pope 2000). Once inhaled, nanoparticles can reach the alveolar region of the lungs and even translocate to other vital organs. They may be more harmful than micrometer (μm)-size particles with the same chemical composition, probably attributed to their large surface area with respect to their size, leading to enhanced interactions with biological fluids and cells (Nel et al. 2006; Li et al. 2003; Oberdörster et al. 2005; Pilou et al. 2015).

Studies to determine the emissions from ME 3D printers are scarce. Stephens and colleagues (2013) carried out a study in workplace conditions and classified the ME 3D printers as high particle emitters. They reported particle emission rates of $3.2 \cdot 10^9$ particles per second ($\# \text{ s}^{-1}$) and $3.3 \times 10^8 \# \text{ s}^{-1}$ for ABS and PLA filaments, respectively, based on modeling. Kim and colleagues (2015) studied aerosol and gaseous emissions from three ME 3D printers that used ABS and PLA and performed their measurements in a chamber. The aerosol emission rates were significantly lower than those of Stephens and colleagues (2013), and the emitted particle mean sizes varied greatly among polymers and 3D printers used. Afshar-Mohajer and colleagues (2015) studied binder jetting technology, showing significant volatile organic compounds (VOCs) and aerosol

emissions. Although the results are not directly comparable, attributable to very distinct technologies, the particles emitted were larger than those emitted by material extrusion, as expected because of dust handling.

The present study aims to characterize particulate emissions covering size resolved data from 1 nm to 31 μm . Volatility measurements were used as an indirect method to infer particle composition and mixing state (chemical diversity among particles). We also measured the gaseous and VOC emissions of a low-end ME 3D printer using the most common plastic polymers in the market. In order to allow a comparison between default and user-defined settings, we also evaluated the influence of the extruder temperature on the emissions. Emission rates were measured in a test chamber and estimated in a full-sized test room under controlled conditions. In the latter, indoor aerosol dynamics modeling was used.

Materials and Methods

3D Printer and Feedstock

The 3D printer used in this study was based on ME technology (miniFactory Oy, Finland, model 3 Education Edition Single Extruder). It represents an affordable AM machine for use at home, offices, or schools for fast prototyping or educational purposes. The plastic filament is fed into the extruder in precise amounts, where it melts and is deposited by a nozzle, layer upon layer, on the heated build platform, also called bed. The printer is equipped with a single nozzle of 0.4 millimeters (mm) in diameter, which allows the use of plastic filaments of 1.75 mm in diameter and deploys layers of material of 0.02 to 0.64 mm in thickness. The temperature settings can be adjusted by the user and range between 40°C and 300°C in the extruder (T_e) and between 40°C and 105°C in the bed (T_b).

The two most common materials used in 3D printers based on ME were selected: ABS (3D printer filament, ABS-1.75 mm, red in color) and PLA (3D printer filament, PLA-1.75 mm, orange in color). ABS is an oil-based, durable, light material and has recommended printing temperatures of $T_e = 230$ to 250°C and $T_b = 80$ to 105°C. PLA is a biodegradable material produced from cornstarch or sugarcane. It is hard and resilient, but less durable than ABS, and its low melting point may cause objects to deform under moderate heating. The recommended temperatures are $T_e = 180$ to 210°C and $T_b = 40$ to 60°C.

The manufacturers of 3D printers often advise the use of several products (e.g., glue, tape, or hairspray) to improve the materials' grip of the bed and thus avoid objects shifting during printing. We did not use any of these products in order to avoid the emission of aerosol or volatile compounds from sources other than the printing material. However, this caused some printing difficulties.

All experiments involved building a small object until the desired operating time was achieved. The ME build cycle was stopped prematurely in cases of visible problems.

Each build cycle consisted of a sequence of operations that varied in time. The printer was previously loaded by feeding the

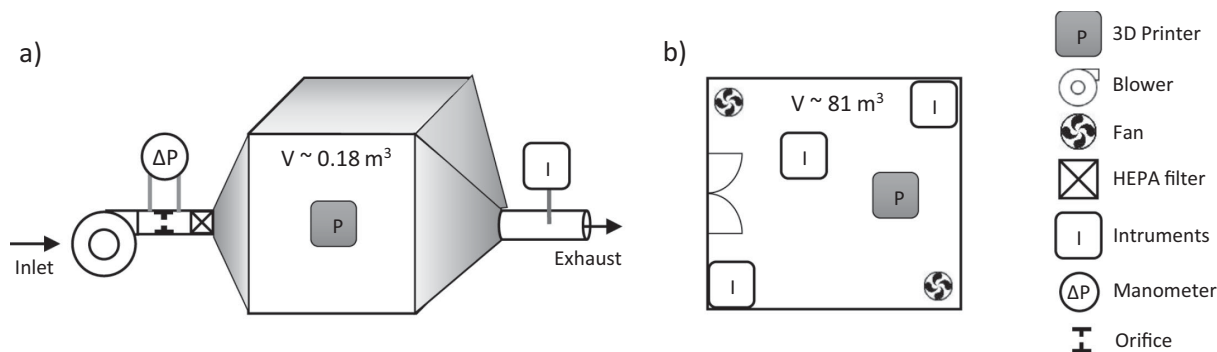


Figure 1 Experimental setup for (a) measurements in test chamber and (b) conventional laboratory room. HEPA = high-efficiency particulate arrestance; m^3 = cubic meters.

polymer into the extruder. Following the 3D data processing, the printer started heating the bed until the set point temperature was reached. After this, extruder heating began, and as soon as the desired temperature was reached, the actual printing started. The T_e during the ABS prints were 230, 238, and 250°C, whereas T_b was kept at 90 or 110°C. PLA printing was done with T_e at 200 and 230°C and T_b at 70°C. These temperatures represent scenarios of default and customized settings that may exceed recommended temperatures.

Measurement Setup and Instruments

The measurements were performed in two distinct environments: an emission test chamber and a conventional laboratory room, and both real-time and offline analytical techniques were used in order to fully characterize aerosol, gaseous, and VOC emissions.

Measurement Setup

The use of a chamber allows measuring particle and gas emission rates directly with negligible background levels and relate them to the several phases of the ME build cycle, given that the residence time of the emitted species in the chamber is very short. Further, the measurement of trace gases is enhanced attributable to the low dilution rate.

We used a stainless steel chamber with a volume of approximately 0.18 cubic meters (m^3) (figure 1). A blower provided the desired airflow to the chamber through stainless steel tubing. The airflow rate was set to $0.014 \text{ m}^3 \text{ s}^{-1}$ using a calibrated critical orifice. Thus, the nominal residence time in the measurement system was approximately 13 s. The air passed through a high-efficiency particulate arrestance (HEPA) filter in order to remove any background concentration of particles. The sampling probes of all the instruments were placed at the outlet of the chamber.

Humidity and temperature were measured by an MI70 measurement indicator with an HMP75 probe (Vaisala, Vantaa, Finland). During the printing, the average air temperature was 28°C and the relative humidity varied between 20% and 32% inside the chamber.

The second measurement setup was based on a test room of a conventional building under controlled conditions. This

experiment simulates conditions in a well-ventilated room, with low background concentrations of pollutants. It allows to assess the user's exposure to gas and particle emissions. Particles emission rates were based on modeling, which is commonly applied to indoor environments (Hussein and Kulmala 2008).

The test room had a floor area of 27 m^2 , the volume was approximately 81 m^3 , and the surfaces were made of stainless steel and glass. The incoming air (flow rate approximately $0.115 \text{ m}^3 \text{ s}^{-1}$) was filtered from gases and particles, resulting in a background particle number concentration of approximately 300 particles per cubic centimeter ($\# \text{ cm}^{-3}$). The air exchange rate was estimated to be approximately 5 per hour (h^{-1}). The average temperature and relative humidity in the room ranged between 24 and 28°C, and 24% and 38%, respectively.

The printer was placed near the center of the room on a table (height = 74 centimeters). Two tabletop fans at opposite corners of the room provided convective mixing of the room air. Most instruments were positioned underneath the room ventilation shaft, whereas two portable particle counters (DiSCmini) were placed at two opposite corners of the room to assess the homogeneity of the aerosol in the room.

Particle Measurements

Two scanning mobility particle sizers (SMPS) were used to obtain the particle number size distribution in the ultrafine size range: a TSI 3080N classifier coupled with the Ultrafine Condensation Particle Counter (UCPC model 3776; TSI Inc., Shoreview, MN, USA) and a Grimm SMPS+C (series 5.400; Grimm Aerosol Technik GmbH, Ainring, Germany). The TSI SMPS measured in the size range of 2.02 to 63.8 nm and 4.45 to 140.7 nm, depending on the inlet flow selected, and the Grimm SMPS measured particles in the size range between 5.5 and 350 nm. These devices classify particles according to their mobility equivalent diameter (D_p) with a high size resolution and accuracy and were operated with a time resolution of 3 minutes. A Particle Size Magnifier (PSM model A11nCNC; Airmodus Oy, Helsinki, Finland) was used to measure aerosol particles in the size range 1 to 3 nm (Vanhanen et al. 2011). During measurements in the chamber, the air was sampled through conductive sampling lines, to avoid electrostatic losses except in case of DiSCmini and PartectorTEM when Teflon tubing was used

instead. The data of SMPS and PSM systems were corrected for diffusional losses occurring in the sampling lines (Hinds 1999).

The total particle concentration was measured in real-time by a condensation particle counter (CPC; TSI model 3007) in the size range of 0.01 to 1 μm and by two portable DiSCmini devices (Matter Aerosol AG, Wohlen, Switzerland), in the size range 0.01 to 0.7 μm (Fierz et al. 2011). A portable PartectorTEM (NANEOS, Windisch, Switzerland) measured the real-time lung deposited surface area (LDSA) for particles of 0.01 to 10 μm in diameter (Fierz et al. 2014). The LDSA has been increasingly considered as one of the parameters correlating better with aerosol toxicity (Jung and Kittelson 2005).

The volatility and mixing state of emitted nanoparticles were assessed using a volatility tandem differential mobility analyzer (VTDMA) described by Mendes and colleagues (2015). This instrument selects particles of a single size (monodisperse) and exposes them to high temperatures in a thermodenuder, assessing their behavior upon heating with respect to a change in size and number concentration. The VTDMA was operated in temperature scanning mode, exposing monodisperse particles ($D_p = 15 \text{ nm}$) to temperatures between 60 and 230°C. The PSM was also coupled with the thermodenuder to assess the existence of refractory cores with diameter larger than 1.2 nm.

Transmission electron microscopy samples were collected onto copper grids (200 mesh) coated with holey carbon film (EMS, CF200-Cu). The grids were placed, depending on the sampling location, on polycarbonate filters in air sample cassettes or on PartectorTEM sample holders. The samples were analyzed using a transmission electron microscope (TEM; JEM 1220; Jeol, Ltd., Tokyo, Japan).

Gaseous Compounds

The selected gaseous compounds of the thermal degradation of polymers, that is, carbon monoxide (CO), nitrogen oxides (nitrogen monoxide [NO], nitrogen dioxide [NO₂]) and hydrogen cyanide (HCN) were measured using portable multigas Dräger X-am 5600 Monitors with IR-sensors (Dräger Safety AG & Co. KGaA, Lübeck, Germany). Carbon dioxide (CO₂) was measured using a MI70 measurement indicator with a GMP70 (Vaisala) probe. We used a photoionization detector (ppbRAE 3000 PGM-7340; RAE Systems Inc., San Jose, CA) with an ultraviolet lamp of 10.6 electron volts to track the variation of different volatile gaseous compounds.

Formaldehyde was sampled with a flow of 1 liter per minute (L min^{-1}) into a SepPak C18 sampler coated with 2, 4-dinitrophenylhydrazine and assayed with liquid chromatography. Activated carbon tubes (SKC 226-01) were used for sampling with a flow of 0.05 L min^{-1} , and gas chromatography for analyzing 1,3-butadiene. To determine the concentration level, we used pure reference compounds.

VOCs were collected into a Tenax TA Carbograph 5TD adsorbent tube with a flow of 0.1 L min^{-1} and were analyzed using gas chromatography. Thermodesorption and mass selective detector, Wiley and NIST libraries, and pure reference substances were used for qualitative and quantitative analysis. Total VOC (TVOC) contains substances that are between

n-hexane and n-hexadecane on the chromatogram and are reported as a toluene equivalent.

We collected particulate matter into a Teflon filter with a flow of 2 L min^{-1} and analyzed these using infrared spectroscopy. Different hydrocarbons (heptane, paraffin) were used as reference compounds.

Particle Emission Rate

During chamber tests, it was reasonable to assume that a homogenous concentration within the chamber would result from turbulent mixing. The high flow inside the chamber assured that the aerosol concentration measured corresponded to fresh emissions, which arise from different ME build cycle phases. When the flow rate is known, the particle emission rate, S , is given by equation (1):

$$S = NQ \quad (1)$$

where N is the total particle number concentration and Q is the chamber inlet flow rate. The concentrations were corrected for diffusional particle losses in the sampling lines by the following formula (Kulkarni et al. 2011) (equation 2):

$$\eta = \exp[-\xi Sh] \quad (2)$$

where η is the particle penetration efficiency through a tube under laminar flow, ξ is a diffusion parameter (dimensionless), and Sh is the Sherwood number, a dimensionless mass transfer coefficient, which is a function of the diffusive deposition velocity.

We used a simple aerosol model for obtaining particle emission rates during the experiments in the room. The evolution of the particle number size distribution is described by the balance equation (Hussein and Kulmala 2008). Assuming that the particle concentration in the incoming air was negligible, we used the following balance equation (equation 3):

$$\frac{dN_i}{dt} = -(\lambda + \beta_i)N_i + S_i + J_{coag,i}, \quad (3)$$

where N_i is the number concentration of particles in size section i , t is time, λ is the ventilation rate, β_i is the deposition rate, S_i is the source (printer emissions), and $J_{coag,i}$ is the change rate attributed to coagulation. $J_{coag,i}$ was calculated on the basis of the measured particle number size distribution and the theory of Seinfeld and Pandis (2006). Assuming that λ and β stay constant, the integration over a time interval and subsequent division by the length Δt of this time interval gives (equation 4):

$$\frac{\Delta N_i}{\Delta t} = -(\lambda + \beta_i)\overline{N_i} + \overline{S_i} + \overline{J_{coag,i}}, \quad (4)$$

where the overlines denote means for the given time interval. For periods without emissions (i.e., $S = 0$) we have (equation 5):

$$\lambda + \beta_i = \frac{-\Delta N_i / \Delta t + \overline{J_{coag,i}}}{\overline{N_i}}. \quad (5)$$

We assumed that $S = 0$ when the printer was off, except for the first couple of minutes after printing ended. We applied equation (5) for time intervals a few minutes after the printing ended and lasting a few tens of minutes. After obtaining $\lambda + \beta_i$, we applied equation (4) to the printing periods in order to obtain the mean emission rates, \bar{S}_i .

Dilution Ventilation Air Flow Rate

Based on the mass balance equation of the room, the time dependence of the contaminant concentration can be estimated using the well-mixed equation (equation 6):

$$c(t) = \frac{m}{Q} (1 - e^{-\frac{Q}{V}t}) \quad (6)$$

where m is the emission rate, Q is the air flow rate of the room, t is time, and V is the room volume. This equation states that the concentration is exponentially increasing while emission is continuing and is asymptotically approaching the steady-state concentration, $c(\infty) = \dot{m}/Q$. Steady-state concentration can be assumed to be the maximum average concentration of the room. This can be used to estimate the air exchange rate of the room. However, the incomplete mixing within the room is normally taken into account using an appropriate coefficient. Thus, the simple equation for estimating the air flow rate, Q , required to dilute the contaminant emitted at a rate m to the desired reference concentration C_{ref} and assuming incomplete mixing with the factor of k (equation 7).

$$Q = k \frac{\dot{m}}{C_{ref}} \quad (7)$$

Results

Particulate Emissions

Chamber Measurements

Although aerosol was measured in a large size range, only the nanoparticle range revealed significant particle emission. We measured aerosol mass concentrations below limit of quantification (LOQ) (LOQ = 0.07 milligrams m^{-3}) for both materials studied.

Figure 2 shows the particle total number concentration during six printing events; four prints using ABS (figure 2a to 2d) and two prints using PLA (figure 2e and 2f). The color map of size resolved particle number concentration was obtained from the TSI SMPS data in most printing events and was merged with Grimm SMPS+C data in the event PLA-1 (figure 2e). The average particle size distributions are shown in figure S1 of the supporting information available on the Journal's website.

A burst of nanoparticles was detected when the extruder reached the melting point of the material. After this, the concentration stabilized during printing. The mechanical moving parts of the printer produced no significant particle emissions. The emissions before and after printing can be considered

negligible, although we observed few particles entering the chamber and/or instruments noise.

The effect of printer malfunction on the aerosol concentration and size distribution is shown in figure 2a after 65 minutes: A strong increase in particle number concentration, increase of the mean particle size from 8.8 to 15.5 nm, and a broadening of the size distribution up to 100 nm were observed. The printing event ABS-3 ($T_e = 238^\circ\text{C}$; figure 2c) was also affected by some remaining ABS residues on the nozzle surface, explaining the larger particle size and higher particle emission than that in the event ABS-4 ($T_e = 250^\circ\text{C}$; figure 2d). PLA printing at $T_e = 200^\circ\text{C}$ released some particles at the beginning (figure 2e), but the emission rapidly decreased to negligible values. The PSM showed a significant emission of particles with size smaller than 3 nm throughout the event. PLA printing at $T_e = 230^\circ\text{C}$ (figure 2f) showed a great increase in particle emission, reaching the values obtained with ABS at similar temperature. A sudden temperature decrease in the extruder after 40 minutes resulted in a drastic decrease in particle emission. It must be noted that 200°C is the maximum extruder temperature recommended for PLA, and higher temperature was used for testing purposes only.

The estimation of the total concentration for particle emission rate was based on SMPS measurements, given that this was the only instrument that covered the size range and concentration of emitted particles.

Table 1 summarizes the particle emission rate, particle size distribution, and concentration statistics based on SMPS measurements. Printing event ABS-1 was divided into two events: ABS-1a, which refers to the first period of printing (minutes 15 to 65) when the printer process was according to operational procedures, and ABS-1b, referring to the second period (minutes 65 to 120) when the misplacement of the material caused charring of ABS in the outer surfaces of the nozzle.

Room Measurements

Figure 3 displays the particle number concentrations measured by the SMPS, PSM, CPC, and both DiSCmini monitors, in addition to particle size distribution measured by the SMPS. The background particle number concentration was below $300 \# \text{cm}^{-3}$ and was mostly composed of particles larger than those emitted during the printing events. The DiSCmini devices, which measured similar particle concentrations at opposite corners of the room, confirmed that the air was well mixed.

During the four ABS prints (ABS-5 to ABS-8), the particle concentration reached values above $10^4 \# \text{cm}^{-3}$. In order to estimate emission rates based on indoor aerosol modeling, the concentration decay after each of these four periods was used to estimate the decay rate, $\lambda + \beta$, and the result is shown in figure 4. Concentrations of particles smaller than 6 nm show a high uncertainty, and we decided not to estimate their decay rate. Only printing event ABS-5 produced a substantial number of particles larger than 20 nm. The estimate of $\lambda + \beta$ after this printing event was mainly based on the decay of this size range. We calculated the emission rates for five of the six printing periods seen in figure 3. Because printing event PLA-3 produced very few particles, the model assumptions were not

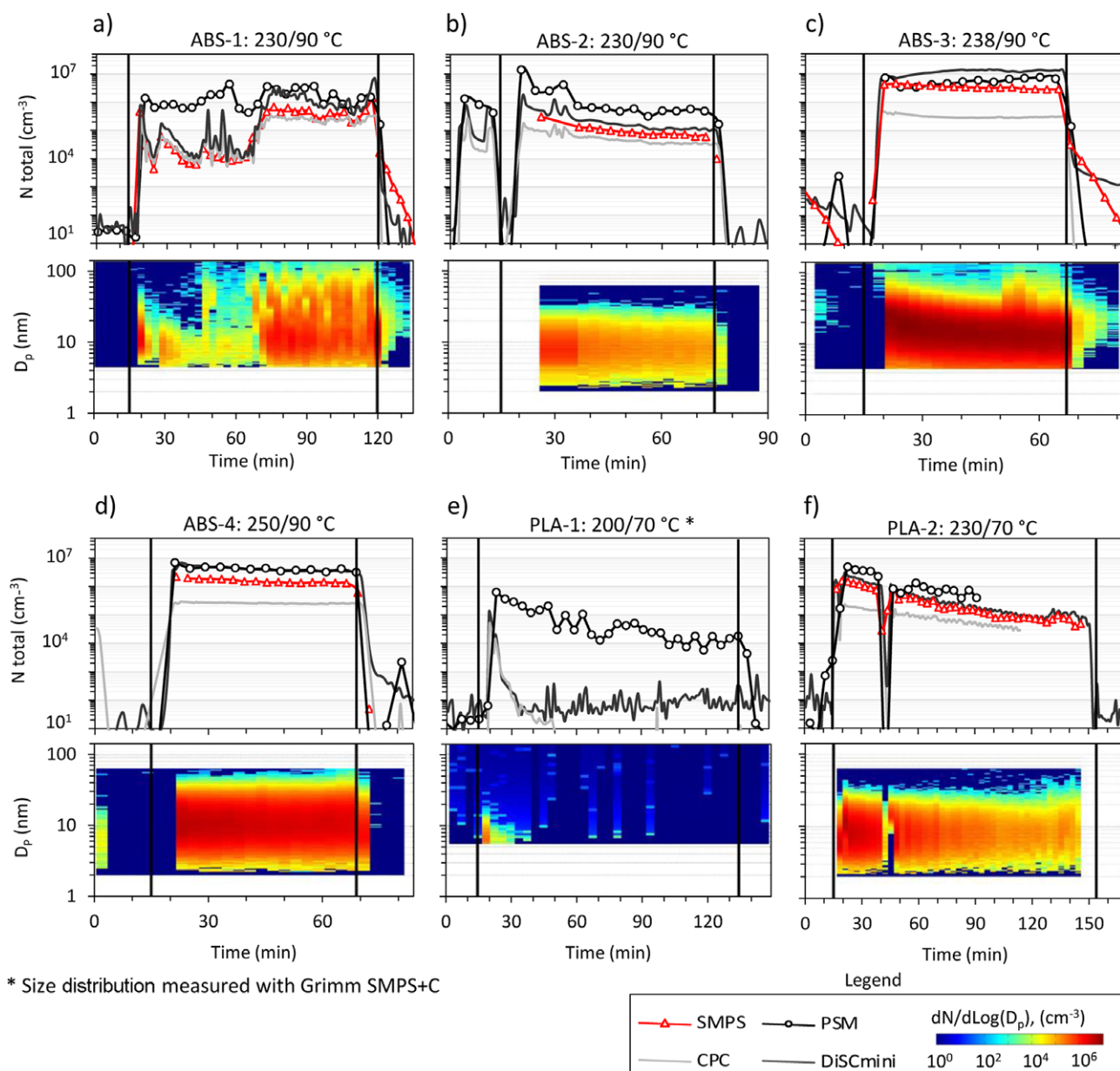


Figure 2 Total particle number concentration (N) during printing events in chamber experiments and corresponding particle number size distribution. Acrylonitrile-butadiene-styrene (ABS) printing at (a and b) T_e/T_b of 230/90°C, (c) 238/90°C and (d) 250/90°C and polylactic acid (PLA) printing at (e) T_e/T_b of 200/70°C and (f) 230/70°C. The vertical lines define the printing period, from heating the bed to stop printing. SMPS = scanning mobility particle sizers; PSM = particle size magnifier; CPC = condensation particle counter; DiSCmini = portable particle counter; T_e = temperature of extruder; T_b = temperature of bed; nm = nanometers; cm^{-3} = per cubic centimeter; $dN/d\text{Log}(D_p)$, (cm^{-3}) = Normalized particle number concentration per cubic centimeter, in logarithmic scale.

met and the event was not considered. Printing event ABS-5 was divided into two sections: ABS-5a, which refers to normal operating conditions, and ABS-5b, which identifies the printing period under malfunction conditions. Figure 4b shows the size-resolved emission rates for the simulated printing periods. Table 2 summarizes the results that characterize the emissions in the room. In addition to the modeled mean particle emission rate, we also present the particle concentration and parameters that describe the size distribution.

Particle Volatility and Morphology

The results from the VTDMA show that the selected particles with $D_p = 15$ nm were essentially volatile. Figure 5 shows the remaining number and volume fractions of selected particles after heating in the thermodenuder. ABS particles had fully evaporated beyond detection at 200°C and PLA particles at 160°C. Particles from both materials suffered gradual volume loss as temperature increased, indicating the presence of compounds of high and low volatility. The analyzed aerosol was

Table 1 Nanoparticle statistics for chamber measurements

Event	T_e/T_b (°C)	N (# cm^{-3})	S (# s^{-1})	GMD (nm)	GSD	LDSA ($\mu\text{m}^2 \text{cm}^{-3}$)	Observations
ABS-1a	230/90	$2.6 \cdot 10^4$	$3.7 \cdot 10^8$	8.8	1.38	16	Standard temperature
ABS-1b	230/90	$4.4 \cdot 10^5$	$6.2 \cdot 10^9$	15.5	1.77	350	Malfunction
ABS-2	230/90	$9.8 \cdot 10^4$	$1.4 \cdot 10^9$	7.9	1.56	33	Standard temperature
ABS-3	238/90	$2.8 \cdot 10^6$	$3.9 \cdot 10^{10}$	12.8	1.45	2433	ABS residues in nozzle
ABS-4	250/90	$1.5 \cdot 10^6$	$2.2 \cdot 10^{10}$	10.5	1.56	518	High temperature
PLA-1	200/70	$7.4 \cdot 10^{2a}$	$1.0 \cdot 10^{7a}$	—	—	3	Standard temperature
PLA-2	230/70	$3.7 \cdot 10^5$	$5.2 \cdot 10^9$	7.9	1.53	62	High temperature

Note: Total number concentration (N), emission rate (S), geometric mean diameter (GMD), and geometric standard deviation (GSD) based on SMPS data, except event PLA-1. LDSA values measured by the PartectorTEM. The values represent the average of the printing period of each event.

^aParticle concentration and emission rate based on condensation particle counter measurements.

T_e = temperature of extruder; T_b = temperature of bed; ABS = acrylonitrile-butadiene-styrene; PLA = polylactic acid; # cm^{-3} = particles per cubic centimeter; # s^{-1} = particles per second; LDSA = lung deposited surface area; $\mu\text{m}^2 \text{cm}^{-3}$ = square micrometers per cubic centimeter of air.

shown to be internally mixed, meaning that all particles appear to behave similarly upon heating, and suggesting similar composition and origin for all the particles sampled. Because the VTDMA had a lower detection limit of 5 nm, we also investigated the existence of remaining refractory cores larger than 1.2 nm by coupling the PSM and the thermodenuder during the test PLA-2. The results indicate that no refractory cores remain after heating at 250°C. Figures S2 and S3 in the supporting information on the Web complement the results presented here.

We collected several TEM samples during the printing events. The TEM analysis of the samples showed very little number or none detectable particles within the resolution of the analysis in the samples and did not allow further conclusions.

Gaseous Compounds Emissions

During the chamber tests, the average concentration of CO_2 varied between 405 and 482 parts per million (ppm). There was no clear relation between CO_2 concentration and the heating of the extruder or the printing. We detected no other selected decomposition compounds (CO , NO , NO_2 , and HCN) or butadiene when printing with ABS (not measured when printing with PLA). Traceable amounts of formaldehyde, acetaldehyde, and acetone were observed in both ABS and PLA printing. The measured formaldehyde concentrations varied between 2 and 3 $\mu\text{g m}^{-3}$, corresponding to an emission rate between 30 and 40 nanograms (ng) s^{-1} . We observed no significant difference between the aldehyde concentrations emitted from the printing materials. The TVOC concentration ranged from 230 to 270 $\mu\text{g m}^{-3}$ and was at the chamber's background level. Some minor fluctuations in VOC concentrations were measured occasionally, but they were not linked to printing events. Although we measured a small concentration of VOCs, we noticed some qualitative differences between the compounds emitted. ABS printing emitted traceable amounts of styrene (14 $\mu\text{g m}^{-3}$, 200 ng s^{-1}), which were not detected in PLA printing.

We also observed 1-butanol and 2-propanol (included in TVOC concentration), most likely originating from the particle measurement instruments.

During the room studies, we measured the same compounds as those measured during the chamber tests. We detected no gaseous compounds, such as CO , NO , NO_2 , HCN , and 1,3-butadiene, or aerosol mass from the plastic materials. Traceable amounts of formaldehyde at concentrations of 2 to 3 $\mu\text{g m}^{-3}$ were detected, as was also the case in the chamber tests. The TVOC concentrations varied between 250 and 520 $\mu\text{g m}^{-3}$ for both polymers printed. A traceable amount (2 $\mu\text{g m}^{-3}$) of styrene was also detected during ABS printing. The concentration of VOCs measured by ppbRAE slightly increased versus time, but this did not seem to be connected to printing events.

Discussion

ABS emitted a significant number of nanoparticles during the ME build cycles, whereas with PLA, the emission of nanoparticles was not as high. This is in line with previous studies (Kim et al. 2015; Stephens et al. 2013). During normal operating conditions, the nanoparticle emission rate from ABS printing ($T_e = 230^\circ\text{C}$) varied between $3.7 \cdot 10^8$ and $4.0 \cdot 10^9$ # s^{-1} , with an average of $1.9 \cdot 10^9$ # s^{-1} . While printing with PLA, using the recommended settings ($T_e = 200^\circ\text{C}$), the measured particle emission rate was much lower: $1.0 \cdot 10^7$ to $6.0 \cdot 10^7$ # s^{-1} . Stephens and colleagues (2013) estimated, based on modeling, particle emission rates of $3.2 \cdot 10^9$ # s^{-1} for ABS ($T_e = 220^\circ\text{C}$) and $3.3 \cdot 10^8$ # s^{-1} for PLA ($T_e = 200^\circ\text{C}$). These values agree with ours regarding ABS, but are higher for PLA filament. Kim and colleagues (2015) reported emission rates for ABS printing at 250°C and PLA at 210 to 220°C of $2.7 \cdot 10^9$ # s^{-1} and $7.7 \cdot 10^6$ # s^{-1} , respectively, based on chamber measurements. These values are somewhat lower than ours are, but the particle size range measured by Kim and colleagues (2015) was more narrow, and newly formed nanoparticles may adhere to the surface of background aerosol. A direct comparison between studies is

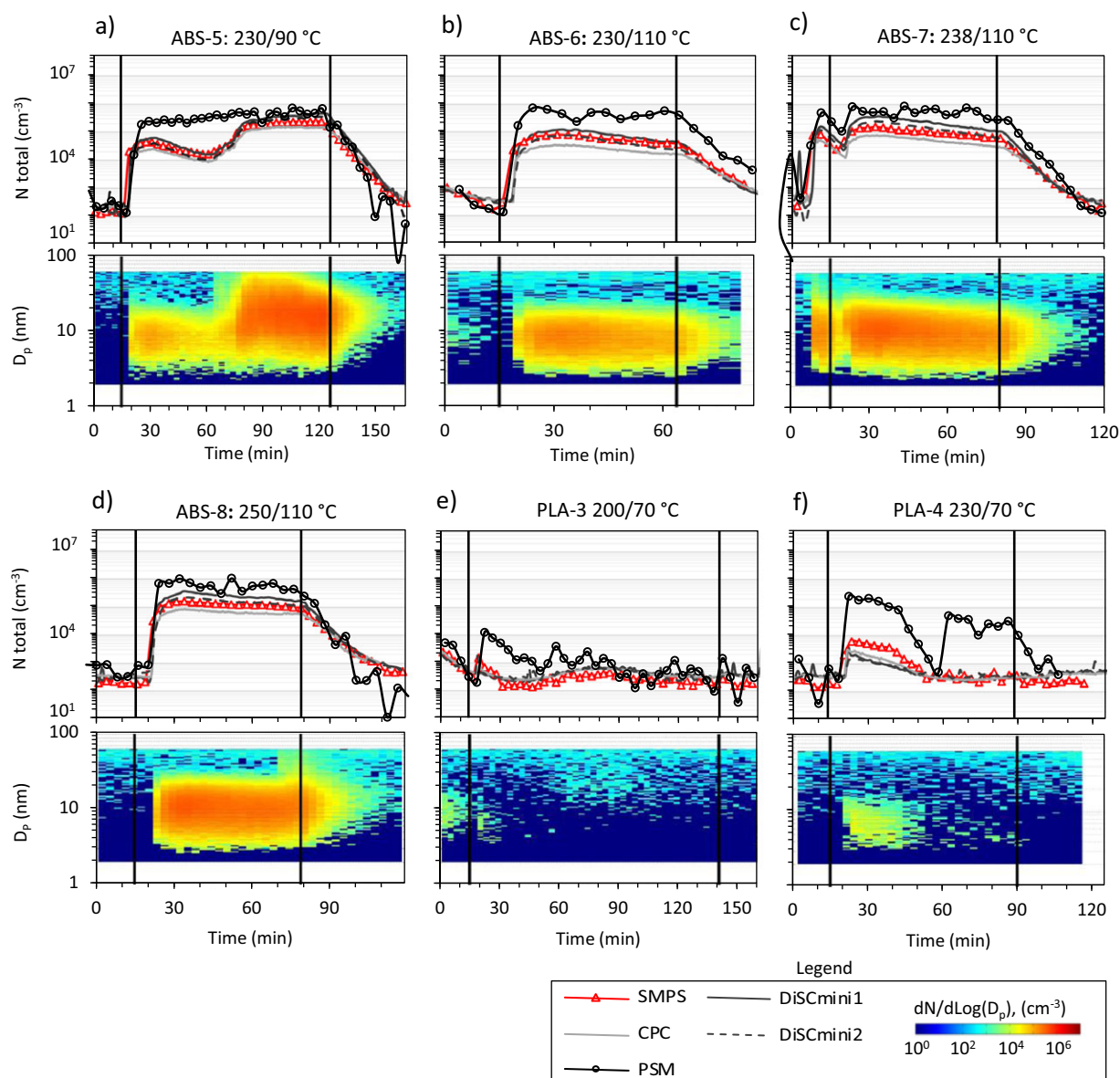


Figure 3 Total particle concentration (N) during printing events in room experiments and corresponding number size distribution obtained by SMPS. Acrylonitrile-butadiene-styrene (ABS) printing at (a) T_e/T_b of 230/90°C, (b) of 230/110°C, (c) 238/110°C, and (d) 250/110°C and polylactic acid (PLA) printing at (e) T_e/T_b of 200/70°C and (f) 230/70°C. The vertical lines define the printing period, from heating the bed to stop printing. SMPS = scanning mobility particle sizers; DiSCmini 1 = portable particle counter 1; DiSCmini 2 = portable particle counter 2; CPC = condensation particle counter; PSM = particle size magnifier; T_e = temperature of extruder; T_b = temperature of bed; nm = nanometers; cm^{-3} = per cubic centimeter; $dN/d\text{Log}(D_p)$, (cm^{-3}) = Normalized particle number concentration per cubic centimeter, in logarithmic scale.

challenging, attributable to the many different variables, such as printer models and settings, materials' composition, the environment of measurements, instruments used, and calculation methods. Despite the significant variability of particle emission rates even between similar printing events, there is strong evidence for a positive correlation between particle emission and extruder temperature.

The results from both chamber and room experiments, presented here, draw similar conclusions, with some variability in

the emissions rates. This variability is to be expected, considering the different measurement and calculation approaches, assumptions made for modeling, and particle behavior, given that processes like coagulation may have a significant impact, especially in the chamber.

During high extrusion temperature tests, the emission rate was significantly higher than that using default settings. In the case of ABS printing, when the extruder temperature was increased to 238 and 250°C, the particle emission rate increased,

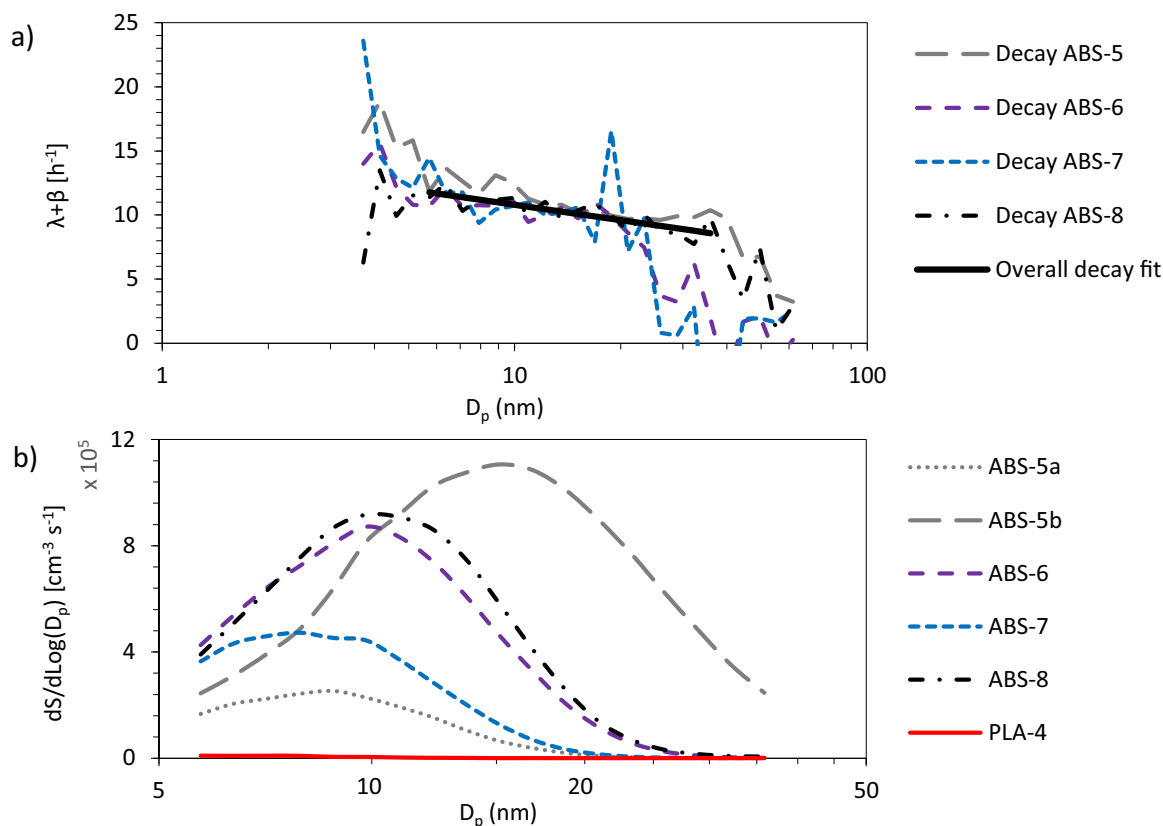


Figure 4 (a) Mean particle concentration decay ($\lambda + \beta$) estimation using equation (4). (b) Mean size resolved emission rates for the given printing events. ABS = acrylonitrile-butadiene-styrene; PLA = polylactic acid; cm⁻³ = per cubic centimeter; s⁻¹ = per second; h⁻¹ = per hour.

on average, ten times to $1.9 \cdot 10^{10} \# \text{ s}^{-1}$. Similarly, in tests using PLA, increasing the extruder temperature to 230°C led to emission rate varying between $6.0 \cdot 10^7$ and $5.2 \cdot 10^9 \# \text{ s}^{-1}$. During malfunction episodes, the particle emission rate reached values up to $3.9 \cdot 10^{10} \# \text{ s}^{-1}$. Malfunction occurred mainly because no additional products were used to increase the adhesion of the built object to the bed. Therefore, in some of the ABS printing events, the object shifted position on the bed and caused sticking of the filament to the nozzle, enabling polymer decomposition attributed to the long exposure to high temperature.

Interestingly, our results on mean particle size differ greatly from those previously reported (Stephens et al. 2013; Kim et al. 2015). Neither of the available studies were carried out in a particle-free environment, and therefore the influence of background aerosols on particle results was significant. Further, we present the first measurements of particles smaller than 10 nm, which was fundamental during our study. Stephens and colleagues (2013) reported peak particle emission at 15 to 49 nm and 48 to 65 nm for ABS and PLA polymers, respectively, whereas Kim and colleagues (2015) reported even larger mean particle sizes; 32.6 nm for ABS and 28 to 188 nm for PLA, which greatly differ from our results of 7.6 to 10.5 nm. Our measurements also show that an increase in the T_c had an influence on the particle mean diameter. For instance, in the room tests, ABS printing at $T_c =$

250°C increased particle GMD from 7.8 to 9.9 nm (27%). The T_b , on the other hand, did not present any influence on aerosol emissions, even at 110°C. The particle size affects directly the particle deposition rate in the different regions of the lungs, and deposition in the alveolar region is enhanced for particles with diameter of approximately 20 nm (ICRP 1994).

Nanoparticle emissions remained negligible during the first minutes of the printing process, when mechanical moving parts operated and the bed heated up. Emission started when the extruder reached operating temperatures (e.g., >200°C). The emission events are characterized by a burst of particles at the beginning followed by a slight decrease until it stabilizes along the printing period. This was also observed by Kim and colleagues (2015) and may occur because of the large amount of polymer melted inside the extruder in a short time period. During printing, particle emission fluctuated slightly in some events, probably attributable to the different amounts of material needs, depending on the complexity of the part and small fluctuations in the extruder temperature. However, the effect of different material feed rates was not within the focus of this study.

In the room tests, ABS particle number concentrations varied between $2.8 \cdot 10^4$ and $5.6 \cdot 10^4 \# \text{ cm}^{-3}$ when recommended printing settings were used. However, if PLA polymer was used, the number concentration in the room did not exceed

Table 2 Nanoparticle statistics for room measurements

Event	T_e/T_b (°C)	N (# cm^{-3})	S (# s^{-1})	GMD (nm)	GSD	LDSA ($\mu\text{m}^2 \text{cm}^{-3}$)	Observations
ABS-5a	230/90	$2.8 \cdot 10^4$	$2.0 \cdot 10^9$	8.2	1.52	15	Standard temperature
ABS-5b	230/110	$1.6 \cdot 10^5$	$1.2 \cdot 10^{10}$	14.0	1.67	345	Malfunction
ABS-6	230/110	$5.6 \cdot 10^4$	$4.0 \cdot 10^9$	7.8	1.52	28	Standard temperature
ABS-7	238/110	$1.1 \cdot 10^5$	$8.0 \cdot 10^9$	9.6	1.54	82	Standard temperature
ABS-8	250/110	$1.2 \cdot 10^5$	$8.0 \cdot 10^9$	9.9	1.51	78	High temperature
PLA-3	200/70	$2.9 \cdot 10^2$	—	26.4	1.97	1	Standard temperature
PLA-4	230/70	$3.4 \cdot 10^3$	$6.0 \cdot 10^7$	7.6	1.81	1	High temperature
Room	—	$2.6 \cdot 10^2$	—	29.0	1.88	1	Background

Note: Total number concentration (N), geometric mean diameter (GMD), and geometric standard deviation (GSD) were based on SMPS data. Particle emission rate (S) was calculated based on equation (3), whereas LDSA was measured by the PartectorTEM. The values represent the averages of each event.

T_e = temperature of extruder; T_b = temperature of bed; ABS = acrylonitrile-butadiene-styrene; PLA = polylactic acid; # cm^{-3} = particles per cubic centimeter; # s^{-1} = particles per second; LDSA = lung deposited surface area; $\mu\text{m}^2 \text{cm}^{-3}$ = squared micrometers per cubic centimeter of air.

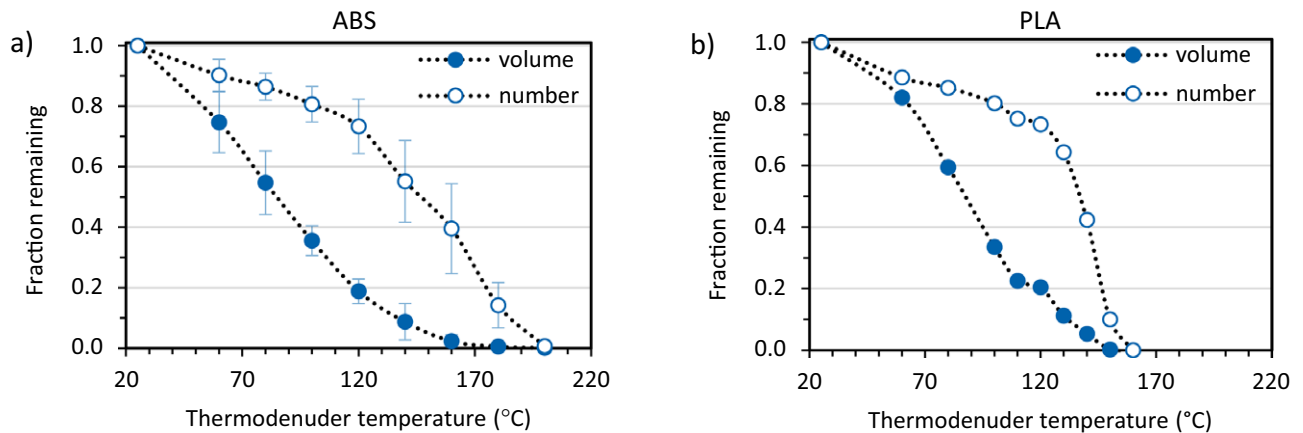


Figure 5 Volatility of monodisperse particles with $D_p = 15$ nm during (a) acrylonitrile-butadiene-styrene (ABS) and (b) polylactic acid (PLA) printing. ABS measurements are shown as an average of all events, whereas PLA refers to one print at $T_e = 230^\circ\text{C}$, during chamber measurements. T_e = temperature of extruder:

the background concentration. If the extruder temperature was increased over the recommended limits, or the printer malfunctioned, the number concentrations were much higher, reaching up to $16 \cdot 10^4$ # cm^{-3} in the case of ABS. A similar effect was observed during PLA printing, with particle concentrations varying from negligible ($T_e = 200^\circ\text{C}$) to more than $3 \cdot 10^3$ # cm^{-3} ($T_e = 230^\circ\text{C}$). The number concentrations in the room were sustained during the ME build cycles, which may take several hours for a single part; thus, the measured durations here are representative for 8-hour exposure and can be used for comparison with (nano reference value; NRV) of $4 \cdot 10^4$ # cm^{-3} (8-hour time-weighted average [TWA]) for bio-persistent nanomaterials of density lower than $6,000$ kilograms m^{-3} (SER 2012). In the case of continuous 8-hour exposure, the number concentrations were well below the NRV in the case of PLA printing, but close to, or slightly higher than, the NRV when ABS was printed using default settings.

Particles in the size range 1 to 3 nm were found in great abundance in all the print cycles, and they were clearly originating from the 3D printing process.

Nanoparticle emission rates from an ME 3D printer measured during our experiments were within the range of those reported for many other indoor activities, including cooking (Buonanno et al. 2009; Géhin et al. 2008; Isaxon et al. 2015) and the use of numerous appliances such as conventional 2D laser printers (He et al. 2010), vacuum cleaners, microwaves, and toasters (Isaxon et al. 2015; Géhin et al. 2008). Nevertheless, particle size, composition, and consequent health implications are expected to be intrinsically different among the several sources.

TEM results were rather inconclusive, attributable to inefficient attachment of particles to the collection substrate. In addition, the emitted particles were very small, further hindering the TEM observations of a limited amount of collected particles.

The VTDMA measurements indicate that the emitted particles were composed of high- and low-volatility compounds, and that no refractory cores were found to exist, even when measuring particle size down to 1.2 nm. All particles were chemically similar (internally mixed), which suggests a common source.

Small concentrations of different volatiles were detected in TVOC analysis, ranging between 250 and 520 $\mu\text{g m}^{-3}$. However, these concentrations were mainly attributed to the emissions from the particle measurement instruments (i.e., 1-butanol and 2-propanol used in the condensation particles counters).

Styrene has a strong smell and may affect the central nervous system. It has been assessed as being possibly carcinogenic to humans (ECHA 2016a). The World Health Organization (WHO) recommends that styrene concentrations in the indoor air are kept below its odor threshold of 70 $\mu\text{g m}^{-3}$ (WHO 2010). During the ABS printing in chamber tests, the concentration of styrene was 14 $\mu\text{g m}^{-3}$ and its emission rate 200 ng s^{-1} . Thus, it is not expected to pose any health risks for persons living or working in the same room, but caution should be taken in the case of using several printers in enclosed rooms.

Formaldehyde is a possible degradation compound of polymers and causes upper respiratory tract and eye irritation and is classified as carcinogenic to humans (ECHA 2016b). The WHO recommends a short-term exposure limit value of 100 $\mu\text{g m}^{-3}$ (WHO 2010). The occupational exposure limit values in different countries for long-term exposure vary between 0.016 and 2 ppm (20 to 2,500 $\mu\text{g m}^{-3}$) (IFA 2015). Traceable amounts of formaldehyde were measured in our study, showing concentrations of 2 to 3 $\mu\text{g m}^{-3}$ for both plastic materials. This is well below the recommended values for formaldehyde.

We used simple mass balance equation (7) to estimate the fresh air flow rate required to dilute the emission down to recommended level. Based on the findings of this study, we assumed that the emission rate is $4 \cdot 10^9 \# \text{s}^{-1}$, the highest observed emission rate during normal ABS printing, and we used the recommended NRV of $4 \cdot 10^4 \# \text{cm}^{-3}$ as a reference concentration. The incomplete mixing was taken into account with the factor $k = 2$. These assumptions produce a required dilution air flow rate of $0.2 \text{ m}^3 \text{ s}^{-1}$. This cannot be typically achieved in homes or regular office rooms. Therefore, it is recommended that containment, such as enclosures and/or local exhaust hoods, is used. Using polymers with lower recommended printing temperatures may reduce emissions significantly. The nozzle and the extruder surfaces should be kept clean, and the printer should be operated at the recommended temperature settings, preferably the lowest value that yields good printing results.

Few studies have been published on 3D printer emissions and many questions remain open. There is a need to investigate emissions dependence on printing polymers quality, as well as toxicological effects of the particles emitted. Further, extending similar emission studies to other materials is of utmost importance, given that new materials enter the market constantly. Printer models and configuration may also play a significant role. Exposure studies should be carried out on printing cafés, schools, and workplaces, where many printers

are likely to be in operation simultaneously during long periods in fairly enclosed spaces. Studies on 3D printer emissions should be also extended to other AM technologies.

Conclusions

This study evaluated emissions from a low-end ME 3D printer, based on gaseous and aerosol components measured in both chamber and conventional room environments. Aerosol measurements were conducted in environments free of background emissions, with particle measurements covering sizes from 1 nm to 31 μm , and the effect of the printing temperature on gases and particle emissions was evaluated.

3D printing produced a significant amount of nanoparticle emissions, when printing with ABS polymer. PLA printing, using the recommended settings, did not produce considerable nanoparticle concentrations. The extruder temperature played an important role in particle emission, with emissions clearly increasing as temperature rose. The malfunction of printers also caused an increase in particle emission and particle size. The mean particle size in our study ranged from 7.8 to 10.5 nm in regular printing, which differs significantly from previous studies. Particles were made of high- and low-volatility compounds, and no refractory cores were observed. Volatile organic and other gaseous compounds were not detected or, if found, were only in traceable amounts, lower than any exposure limit value. Printing polymers differed mostly by the traceable amounts of styrene present during ABS printing.

Following a preventive approach, precautionary measures should be adopted when using 3D printers in nontraditional settings. Although the use of 3D printers is not discouraged, caution must be taken when operating several printers simultaneously, as is normal in most public printing places, schools, or workplaces: Here, the concentration of particles is likely to exceed the indicative value of $4 \cdot 10^4 \# \text{cm}^{-3}$ (8-hour TWA) during long exposure periods.

The material used plays an important role in the overall particle exposure, and we advise keeping the heated sections of the printer clean and use the lower extruder temperatures that yield good printing results. Enclosures, local exhaust ventilation, and air filtering systems can be used to reduce users' exposure to potentially hazardous emissions. Embedding these features into 3D printers during the design phase would certainly produce the best outcome.

Funding Information

This work has been funded by The Finnish Work Environment Fund (grant nos. 114337, 114406, and 114374). This research was included in the collaboration of the FP7 Marie Curie ITN project HEXACOMM (grant no. 315760).

References

- Afshar-Mohajer, N., C.-Y. Wu, T. Ladun, D. A. Rajon, and Y. Huang. 2015. Characterization of particulate matters and total VOC

- emissions from a binder jetting 3D printer. *Building and Environment* 93: 293–301.
- Bradbrook, S., M. Duckworth, P. Ellwood, M. Miedzinski, J. Ravetz, and J. Reynolds. 2013. *Green jobs and occupational safety and health: Foresight on new and emerging risks*. European Agency for Safety and Health at Work. Luxembourg. <https://doi.org/10.2802/39554>. Accessed 28 February 2017.
- Bumgarner, B. 2013. Getting started with a 3D printer. *Make* 12: 12–16.
- Buonanno, G., L. Morawska, and L. Stabile. 2009. Particle emission factors during cooking activities. *Atmospheric Environment* 43(20): 3235–3242.
- Caffrey, T. and T. Wohlers. 2014. 3D printing builds up its manufacturing resume. *Manufacturing Engineering* 152(6): 61–68.
- Dematteo, R. 2011. Chemical exposure and plastics production. National Network on Environments and Women's Health:15. Toronto, Canada. <http://www.cwhn.ca/en/node/45388>. Accessed 13 July 2015.
- ECHA (European Chemicals Agency). 2016a. The brief profile for styrene. *European Chemicals Agency*. <http://echa.europa.eu/fi/brief-profile/-/briefprofile/100.002>. Accessed 10 November 2016.
- ECHA (European Chemicals Agency). 2016b. The brief profile for formaldehyde. *European Chemicals Agency*. <http://echa.europa.eu/brief-profile/-/briefprofile/100.000.002>. Accessed 10 November 2016.
- Fierz, M., C. Houle, P. Steigmeier, and H. Burtscher. 2011. Design, calibration, and field performance of a miniature diffusion size classifier. *Aerosol Science and Technology* 45(1): 1–10.
- Fierz, M., D. Meier, P. Steigmeier, and H. Burtscher. 2014. Aerosol measurement by induced currents. *Aerosol Science and Technology* 48(4): 350–357.
- Géhin, E., O. Ramalho, and S. Kirchner. 2008. Size distribution and emission rate measurement of fine and ultrafine particle from indoor human activities. *Atmospheric Environment* 42(35): 8341–8352.
- He, C., L. Morawska, H. Wang, R. Jayaratne, P. McGarry, G. Richard Johnson, T. Bostrom, J. Gonthier, S. Authemayou, and G. Ayoko. 2010. Quantification of the relationship between fuser roller temperature and laser printer emissions. *Journal of Aerosol Science* 41(6): 523–530.
- Hinds, W. C. 1999. *Aerosol technology*, 2nd ed. New York: Wiley.
- HSE (Health and Safety Executive). 2002. *Controlling fume during plastics processing*. www.hse.gov.uk/copyright.htm. Accessed 13 July 2015.
- Hussein, T. and M. Kulmala. 2008. Indoor aerosol modeling: Basic principles and practical applications. *Water, Air, and Soil Pollution: Focus* 8(1): 23–34.
- ICRP 1994. Human respiratory tract model for radiological protection. ICRP Publication 66. *Ann. ICRP* 24 (1–3): 1–482.
- IFA (Institut Für Arbeitsschutz Der Deutschen Gesetzlichen Unfallversicherungen). 2015. GESTIS international limit values. *Institut Für Arbeitsschutz Der Deutschen Gesetzlichen Unfallversicherungen*. <http://limitvalue.ifa.dguv.de/>. Accessed 8 September 2015.
- Isaxon, C., A. Gudmundsson, E. Z. Nordin, L. Lönnblad, A. Dahl, G. Wieslander, M. Bohgard, and A. Wierzbicka. 2015. Contribution of indoor-generated particles to residential exposure. *Atmospheric Environment* 106: 458–466.
- ISO (International Organization for Standardization)/ASTM (American Society for Testing and Materials). 2015. *ISO/ASTM 52900:2015—Additive manufacturing—General principles—Terminology*, 1st ed. Geneva, Switzerland: International Organization for Standardization.
- Jung, H. and D. B. Kittelson. 2005. Characterization of aerosol surface instruments in transition regime. *Aerosol Science and Technology* 39(9): 902–911.
- Kim, Y., C. Yoon, S. Ham, J. Park, S. Kim, O. Kwon, and P.-J. Tsai. 2015. Emissions of nanoparticles and gaseous material from 3D printer operation. *Environmental Science & Technology* 49(20): 12044–12053.
- Kulkarni, P., P. A. Baron, and K. Willeke, eds. 2011. *Aerosol measurement: Principles, techniques, and applications: Third edition*. Hoboken, NJ, USA: John Wiley & Sons.
- Li, N., C. Sioutas, A. Cho, D. Schmitz, C. Misra, J. Sempf, M. Wang, T. Oberley, J. Froines, and A. Nel. 2003. Ultrafine particulate pollutants induce oxidative stress and mitochondrial damage. *Environmental Health Perspectives* 111(4): 455–460.
- Mendes, L., K. Eleftheriadis, and G. Biskos. 2016. Performance comparison of two thermodenuders in volatility tandem DMA measurements. *Journal of Aerosol Science* 92: 38–52.
- Nel, A., T. Xia, L. Mädler, and N. Li. 2006. Toxic potential of materials at the nanolevel. *Science* 311(5761): 622–627.
- Oberdörster, G., E. Oberdörster, and J. Oberdörster. 2005. Nanotoxicology: An emerging discipline evolving from studies of ultrafine particles. *Environmental Health Perspectives* 113(7): 823–839.
- Pilou, M., O. Mavrofydi, C. Housiadas, K. Eleftheriadis, and P. Papazafiri. 2015. Computational modeling as part of alternative testing strategies in the respiratory and cardiovascular systems: Inhaled nanoparticle dose modeling based on representative aerosol measurements and corresponding toxicological analysis. *Nanotoxicology* 9(s1): 106–115.
- Pope, C. A. 2000. Epidemiology of fine particulate air pollution and human health: Biologic mechanisms and who's at risk? *Environmental Health Perspectives* 108(s4): 713–723.
- Pope, C. A. and D. W. Dockery. 2006. Health effects of fine particulate air pollution: Lines that connect. *Journal of the Air & Waste Management Association* 56(6): 709–742.
- SER (Social and Economic Council). 2012. *Provisional nano reference values for engineered nanomaterials. Advisory report 12/01*. The Hague, the Netherlands: Social and Economic Council. www.ser.nl/~media/Files/Internet/Talen/Engels/2012/2012_01/2012_01.ashx. Accessed 13 July 2015.
- Sims, J., P. A. Ellwood, and H. J. Taylor. 1994. Pollutants from laser cutting and hot gas welding of polymer based materials. In 52nd Annual Technical Conference ANTEC 94. Part 1 (of 3): 1269–1273. San Francisco, CA, USA.
- Stephens, B., P. Azimi, Z. El Orch, and T. Ramos. 2013. Ultrafine particle emissions from desktop 3D printers. *Atmospheric Environment* 79: 334–339.
- Unwin, J., M. R. Coldwell, C. Keen, and J. J. McAlinden. 2013. Airborne emissions of carcinogens and respiratory sensitizers during thermal processing of plastics. *Annals of Occupational Hygiene* 57(3): 399–406.
- Vanhanen, J., J. Mikkilä, K. Lehtipalo, M. Sipilä, H. E. Manninen, E. Siivola, T. Petäjä, and M. Kulmala. 2011. Particle size magnifier for nano-CN detection. *Aerosol Science and Technology* 45(4): 533–542.
- WHO (World Health Organization). 2010. *WHO guidelines for indoor air quality: selected pollutants*. Copenhagen: World Health Organization Regional Office for Europe. www.euro.who.int/__data/assets/pdf_file/0009/128169/e94535.pdf?ua=1. Accessed 13 July 2015.

Supporting Information

Supporting information is linked to this article on the *JIE* website:

Supporting Information S1: This supporting information complements the results discussed in the article. Figure S1 shows the average size distributions of particles emitted during the printing events for both acrylonitrile-butadiene-styrene (ABS) and polylactic acid (PLA) materials in chamber (figures S1a and S1b) and room (figures S1c and S1d) conditions. Figure S2 displays examples of normalized number size distributions of ABS and PLA monodisperse particles after volatilization in a thermodenuder at increasing temperatures. Despite the broadening of the size distribution, one can observe that only one particle mode remains during the heating, indicating the internal mixture of the aerosol analyzed. Figure S3 displays the remaining total number of particles having diameter larger than 1.2 nm after volatilization at several temperatures. This experiment allowed us to verify the inexistence of particulate refractory cores in the size range not covered by the VTDMA system (i.e., below 5 nm).